nature materials

ARTICLES

https://doi.org/10.1038/s41563-020-00900-5

Spontaneous organization of supracolloids into three-dimensional structured materials

Mohammad-Amin Moradi[1,2,3,8], E. Deniz Eren[1,2,3,8], Massimiliano Chiappini[4], Sebastian Rzadkiewicz[1,2], Maurits Goudzwaard[1], Mark M. J. van Rijt[1,2], Arthur D. A. Keizer[1], Alexander F. Routh[5], Marjolein Dijkstra[4], Gijsbertus de With[3], Nico Sommerdijk[1,2,6] ✉, Heiner Friedrich[1,2,3] ✉ and Joseph P. Patterson[1,2,7] ✉

Periodic nano- or microscale structures are used to control light, energy and mass transportation. Colloidal organization is the most versatile method used to control nano- and microscale order, and employs either the enthalpy-driven self-assembly of particles at a low concentration or the entropy-driven packing of particles at a high concentration. Nonetheless, it cannot yet provide the spontaneous three-dimensional organization of multicomponent particles at a high concentration. Here we combined these two concepts into a single strategy to achieve hierarchical multicomponent materials. We tuned the electrostatic attraction between polymer and silica nanoparticles to create dynamic supracolloids whose components, on drying, reorganize by entropy into three-dimensional structured materials. Cryogenic electron tomography reveals the kinetic pathways, whereas Monte Carlo simulations combined with a kinetic model provide design rules to form the supracolloids and control the kinetic pathways. This approach may be useful to fabricate hierarchical hybrid materials for distinct technological applications.

One of the grand challenges in materials science is the organization of matter from the molecular level, through the nano- and mesoscale domains, up to the macroscopic level[1]. Colloidal assembly, which deals with interactions between particles of 1 nm to 1 µm in size[2,3], provides generically applicable strategies for the organization of multiple types of colloids[4,5]. Examples include the use of hydrophilic–hydrophobic interactions[6], electrostatics[7,8] and DNA base pairing[9,10]. These interactions can control the formation of either nanoscale assemblies, which remain stable in solution[9], or meso- to macroscale structures, which form precipitates[6,8,11]. In the absence of the specific interactions mentioned above, colloids can spontaneously organize at high concentrations, driven by entropy. Here spontaneous means that the assembly in three dimensions (3D) occurs in a single step during drying. Spherical particles will typically form face-centred-cubic or hexagonally close-packed lattices[12], which can be controlled through the use of surface templates[13] or spherical confinement[14]. The formation of exotic mesophases through the simple drying of dendritic molecules[15,16] sparked great interest in the role that shape and entropy play in the organization of particles into complex structures at high concentrations[17–21]. Simulations showed that by controlling particle shape, it is possible to spontaneously form a wide range of structures, which include crystals, quasicrystals, liquid crystals and plastic crystals[17,22,23]. Entropy-driven assembly through controlled drying has been extended to the formation of 2D binary[24–28] or ternary[29] nanoparticle superlattices, which in a layer-by-layer approach can be used to make hierarchically structured materials[30]. Open ordered porous materials obtained by mixing binary systems have been reported, in which polymer particle templates are employed for photonic crystals or catalyst supports from oxides like silica or titania[8,31–35]. However, the formation of hybrid materials with a nano- and mesoscale order through the spontaneous 3D hierarchical organization of colloids that consists of two or more components is not achievable through either of these strategies and remains a key challenge in materials science.

In this work, a design strategy is presented in which interfacial chemistry is used to create multicomponent building blocks[6,36] that are dynamic over a wide range of concentrations. The building blocks are supracolloids: hybrid particles formed from a polymer core and a corona of several silica nanoparticles (SNPs). Creating supracolloids by the assembly of nanoparticles around cores through opposite-charge interactions has been discussed[37–39]. At high concentrations (during drying), the supracolloids organize as distinct individual building blocks. During this secondary organization step, the constituent components of the supracolloids spontaneously reorganize and form, driven by entropy, macroscopic materials with a 3D nano- and mesoscale order. Their morphology is determined by the size, shape and interfacial chemistry of the individual component particles, as well as by the dynamic structure of the supracolloid and the entropy-driven reorganization process on drying (Fig. 1a).

Formation and analysis of the supracolloids

We demonstrated this general concept using SNPs (10 and 30 nm) surface functionalized with 3-aminopropyl triethoxysilane (APTES,

[1]Laboratory of Materials and Interface Chemistry and Centre for Multiscale Electron Microscopy, Department of Chemical Engineering and Chemistry, Eindhoven University of Technology, Eindhoven, The Netherlands. [2]Institute for Complex Molecular Systems, Eindhoven University of Technology, Eindhoven, The Netherlands. [3]Laboratory of Physical Chemistry, Department of Chemical Engineering and Chemistry, Eindhoven University of Technology, Eindhoven, The Netherlands. [4]Soft Condensed Matter, Debye Institute for Nanomaterials Science, Utrecht University, Utrecht, The Netherlands. [5]Department of Chemical Engineering and Biotechnology, University of Cambridge, Cambridge, UK. [6]Present address: Department of Biochemistry, Radboud Institute for Molecular Life Sciences, Radboud University Medical Center, Nijmegen, The Netherlands. [7]Present address: Department of Chemistry, University of California, Irvine (UCI), Irvine, CA, USA. [8]These authors contributed equally: Mohammad-Amin Moradi, E. Deniz Eren. ✉e-mail: nico.sommerdijk@radboudumc.nl; H.Friedrich@tue.nl; patters3@uci.edu

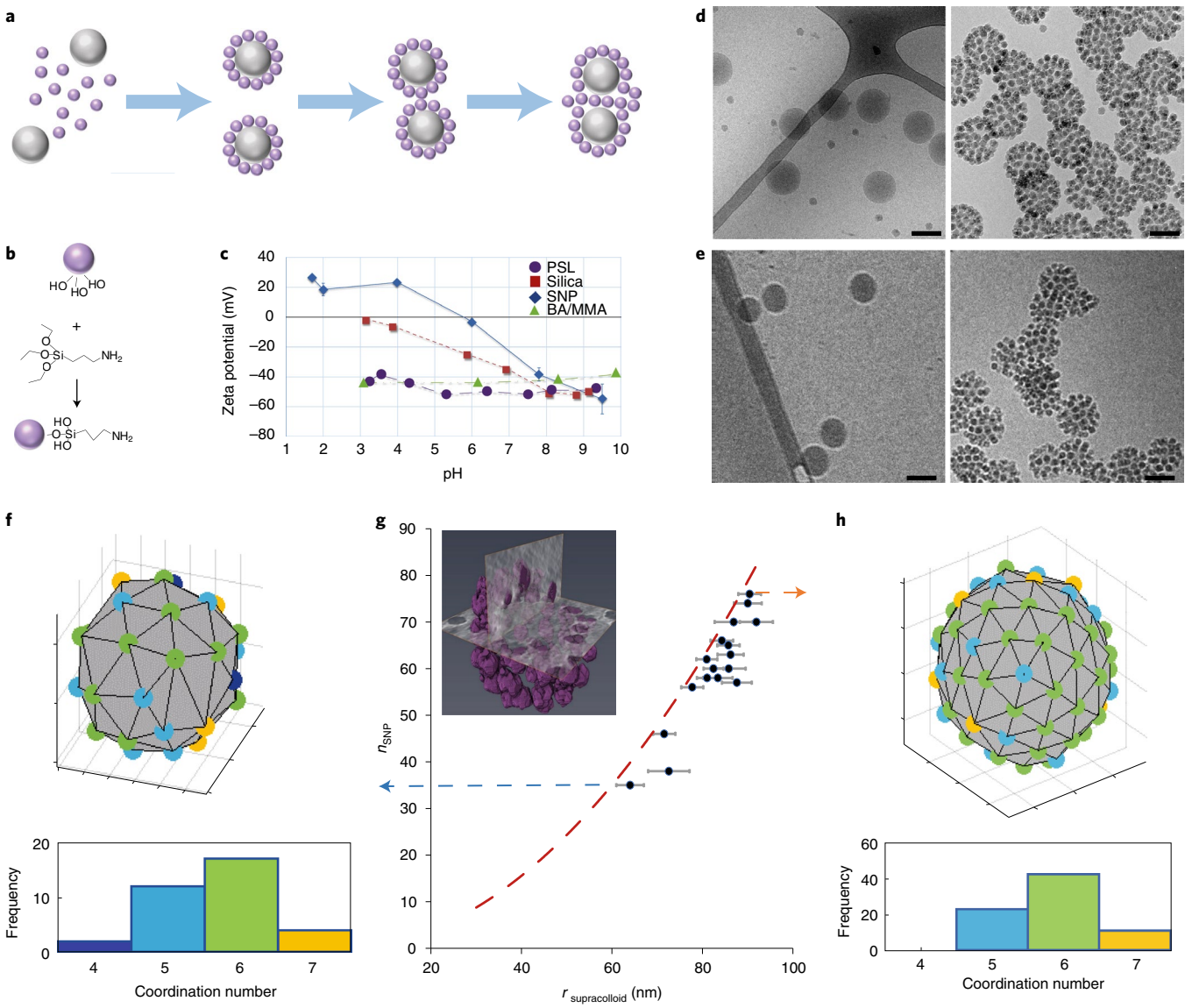

Fig. 1 | Synthesis and self-assembly of the supracolloids. a, Schematic showing the binary assembly strategy for colloidal organization. **b**, Surface functionalization of SNPs. **c**, Plot of the zeta potential of SNPs and PSL spheres versus pH, showing that at low pH there will be a strong attraction between the functional SNPs (1:50 functional group:SNP) and PSL particles. The error bars represent the standard deviation in the mean for three measurements. **d**, CryoTEM images of mixtures of 30 nm SNPs and 100 nm PSL spheres at pH 10 (left, not assembled) and pH 2 (right), showing that at a low pH the SNPs form a close-packed structure on the surface of the PSL spheres. **e**, CryoTEM images of mixtures of 30 nm SNPs and 100 nm BA/MMA spheres at pH 10 (left, not assembled) and pH 2 (right), which show that at a low pH the SNPs form a close-packed structure on the surface of the PSL spheres (for BA/MMA and SNP supracolloids, see Supplementary Figs. 7–9). **f**,**h**, Analysis of the dispersity of the SNP nearest-neighbour network on the surface of a 100 nm (**f**) and a 150 nm (**h**) PSL sphere covered by nominal 30 nm SNPs. **g**, Plot of the number of SNPs on the surface of a single PSL sphere (n_{SNP}) versus the supracolloid radius ($r_{supracolloid}$) with the blue and orange arrows corresponding to the examples shown in **f** and **h**, respectively. The range of the supracolloid radius is due to its natural dispersity and the error bars indicate the standard deviation in the mean according to the procedure for determining the radius. The maximally achievable coverage of a larger sphere by smaller spheres based on Mansfield[50] is shown as the red dashed line in **g**.

pK_a ~7) (Fig. 1b), polystyrene latex (PSL) spheres (100, 140 and 170 nm) with sulfonic acid surface groups (pK_a ~1) and butyl acrylate/methyl methacrylate (BA/MMA) spheres of 80 nm synthesized using starved-feed emulsion polymerization with equal wt% monomers in 1 wt% SDS (surfactant), Na_2CO_3 (buffer) and 0.25 wt% potassium persulfate (initiator) solution. Zeta potential measurements over a range of pH values show that at a high pH both component particles display a negative charge, whereas at a low pH the SNPs become positively charged due to protonation of the surface amines (Fig. 1c). To create our supracolloids, we mixed solutions of SNPs with PSL spheres in a range of pH values, ionic strengths, particle concentrations and particle number ratios (Supplementary Tables 1 and 2). Cryogenic transmission electron microscopy (cryoTEM)[40] was used to qualitatively assess the formation of the supracolloids (Fig. 1d,e and Supplementary Figs. 1 and 2). At pH > 7, the SNP and PSL particles remained separated, whereas at pH < 5, particles assembled into discrete multicomponent supracolloids. Under specific conditions (APTES to silica 1:50, ionic strength 0.3 mM, pH ~2–3), it was possible to create supracolloids with SNPs that fully covered the surfaces of the PSL spheres (Supplementary Fig. 3).

After optimizing the assembly conditions, cryogenic electron tomography (cryoET) was performed to quantitatively analyse the spatial organization of the SNPs on the PSL surface (Fig. 1f–h and Supplementary Figs. 4 and 5). For spheres to form a close-packed structure on a surface it is essential to avoid irreversible random sequential absorption[41], which requires a detailed balance of absorption–desorption and particle hopping. On a flat surface spheres will pack, driven by entropy, into a six-coordinate arrangement. This is not possible on a curved surface, so spheres must pack into a mixed six and non-six coordinate arrangement[42]. Euler proposed that the spheres with non-six coordination numbers (c) can be considered as point defects, characterized by a disclination charge q, where $q = 6 - c$ (ref. [43]). Bausch et al. showed that as the particle size ratio increases, these point defects become too energetically costly and linear arrays of disclinations or 'grain boundaries' are formed instead; here the size ratios were below these at which grain boundaries should form[43,44]. The SNPs packed into a mixture of four, five, six and seven coordinate arrangements in which the total number of SNPs and the coordination numbers depended on the particle sizes and size ratios (Fig. 1f–h and Supplementary Fig. 6). For every supracolloid examined, the mean radius and its associated standard deviation were calculated by averaging the distance of each SNP centroid (extracted from electron tomography data) from the calculated centre of the supracolloid.

Formation and analysis of the 3D structured materials

To organize the supracolloids at high concentrations into hierarchically structured materials, solutions were dried on a variety of substrates (amorphous carbon, silicon wafers and glass slides) under a range of temperatures (4, 7, 10, 18 and 22 °C), and a range of relative humidities (60, 65, 75, 95 and 99%). In some cases, the supracolloid samples contained excess SNPs (Fig. 2c–f, top row); however, during drying, the excess SNPs separated from the supracolloids due to the phenomena of stratification[45], and were typically found at a different locations of the substrate compared with those of the hierarchically structured materials. Moreover, cryoTEM analysis of the supracolloids after centrifuging and removing the free SNPs shows the supracolloids to be intact (extra information is given in the Supplementary Discussion and Supplementary Fig. 10). After drying, a more optimally packed structure arose by reorganization such that a single layer of silica separates the latex particles, and silica particles filled the tetrahedral and octahedral holes of the close packed structure of the supracolloids. The surface of the hybrid assemblies was analysed by scanning electron microscopy (SEM) (Fig. 2 and Supplementary Table 3). Figure 2a–f shows the most ordered structures obtained for each SNP/PSL combination, in which the SNPs formed a dense network around the PSL spheres. After depolymerization at ~500 °C, close-packed structures were still present (Fig. 2a–f, third row) with more or fewer faults, which resulted in somewhat different sixfold fast Fourier transform (FFT) patterns (Fig. 2a–f, fourth row). A summary of domain sizes and wall thicknesses is given in Supplementary Table 4 and Supplementary Figs. 11–14. Volume imaging using focused ion beam SEM (FIB-SEM) tomography (Fig. 2g,h) shows the hexagonal organization of the supracolloids in 3D, which underlines that they, indeed, act as spherical building blocks that organize in 3D at high concentrations, driven by entropy. Close inspection of the internal (Fig. 2i,j) and surface (Fig. 2k,l) structure of the porous SNP network showed that the SNPs reorganized prior to drying to form a close packed (entropically favoured) structure (rewetting disturbs the order (Supplementary Fig. 15)). This can be seen from the filled 'interstitial sites' between the supracolloids (Fig. 2j) and the long-range order observed in the FFT (Fig. 2m) and inverse FFT (Fig. 2n). The FFT showed an arced sixfold pattern, which indicates the SNPs also packed hexagonally with some distortions to the long-range order. The sizes of the domains extended from submicrometre to over tens of micrometres (Supplementary Fig. 16). For the 100 nm PSL-30 SNP and 100 nm PSL-10 SNP combinations, the domain sizes were between 1 and 10 µm, whereas for the combinations that involved the 140 nm PSL and 170 nm PSL, where the droplet surface curvature played a role, the domain size was 10–100 µm, with a depth of about ten layers. Supplementary Fig. 17 shows FIB-SEM lamella images of dried supracolloids as measured by TEM at different tilt angles and the order in the supracolloid and homogeneity in the SNP distribution.

The dynamics between the SNPs and the PSL spheres on the supracolloid surface seems to play a key role in achieving a hierarchical 3D organization by allowing the formation of entropically favoured structures prior to full solvent evaporation. However, the formation of the supracolloids was an essential first step in obtaining well-ordered macroscopic materials. Drying solutions of dispersed particles resulted in disordered or macroscopically phase-separated areas of the individual SNPs and PSL spheres (Supplementary Table 3). This is explained by the phenomenon of colloidal stratification, which describes how particles of different sizes phase separate during drying[45]. In fact, even for solutions that contained highly ordered supracolloids at low concentrations (as analysed by cryoTEM), drying may result in disordered and macroscopically phase-separated materials (Supplementary Table 3).

Analysis of the organization pathways

To investigate the different organization pathways, from highly ordered supracolloids to either ordered or disordered macroscopic materials, time-resolved cryoET was performed during the drying process (Fig. 3 and Supplementary Figs. 18–20). For samples that resulted in disordered structures, we observed the formation of intermediate supracolloid clusters (Fig. 3a,c). These clusters consist of two or more PSL spheres of which the surrounding SNP layers are not preserved due to a rearrangement of the supracolloids from their initial organization in solution. Without this dynamic reorganization, a double SNP layer would always be present between two adjacent PSL spheres (Fig. 3b,d,e). However, in many of the clusters we observed only a single layer of SNPs (Supplementary Fig. 19) or even direct contact between two PSL spheres (Supplementary Fig. 18l). Subsequent to the reorganization clearly demonstrating that supracolloids are dynamic, the PSL:SNP number ratio and the SNP coordination number decrease on further drying due to disassembly and phase separation (Supplementary Fig. 18m). Hence, to form hierarchically ordered hybrid materials, PSL cluster formation should be avoided as this results in the irreversible disassembly of the building blocks in the early stage of drying.

Indeed, for pathways that lead to highly ordered materials we observed that the supracolloids remain separated (that is, no clustering was observed) until they organized into a hexagonal lattice at sufficient high concentrations (Fig. 3d and Supplementary Fig. 20). Importantly, cryoET showed that their PSL:SNP ratio and the SNP nearest-neighbour network was still the same as that for the initial dispersed system at a low concentration (Fig. 3e). This even holds for the situation in which some of the SNPs from neighbouring PSL spheres are within the same distance as those on the same PSL sphere (Supplementary Fig. 20). For the close packing of spheres that have the same charge, the separation distance is dictated by both geometric considerations and electrostatic repulsion between the particles. Consequently, we infer that here the supracolloids were kept apart by the electrostatic repulsion between SNPs on adjacent assemblies. Therefore, this stage of organization represents the most optimal packed structure the supracolloids can form without reorganization. During drying, a more optimally packed structure arises by entropy-driven reorganization in the almost dry state, in such a way that the structure changes from a two-particle to a one-particle silica interlayer between the latex particles. The silica particles probably go into the tetrahedral and octahedral holes, as they cannot move far in the jammed structure (Fig. 3). In support

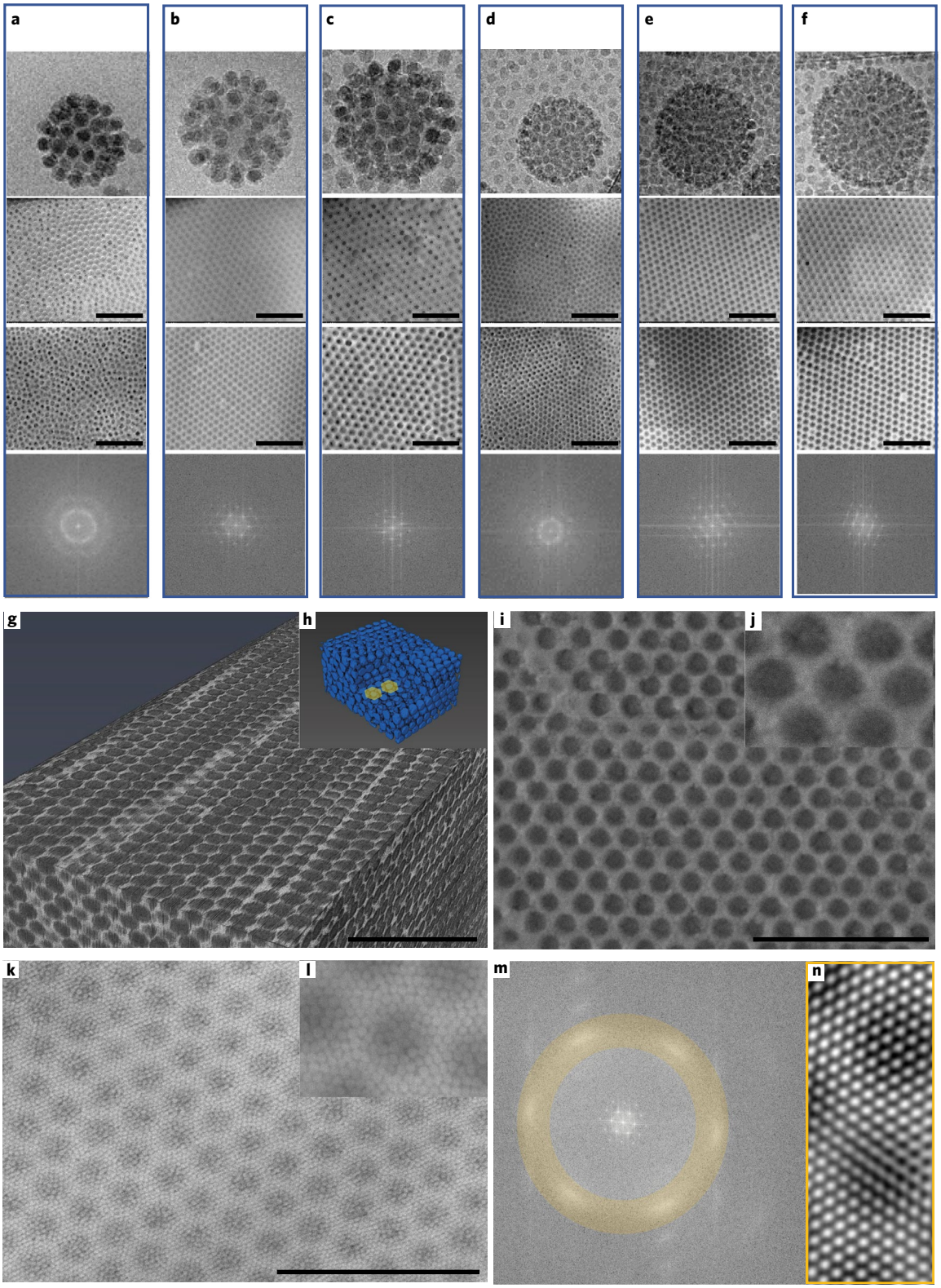

Fig. 2 | Electron microscopy analysis of the macroscopic materials. a–f, The first, second, third and fourth rows show cryoTEM images of the supracolloid, SEM images of the different samples after drying, SEM images after removal of the PSL spheres by depolymerization at 500 °C and the corresponding FFT results of the structures, respectively, of 100 nm PSL, 30 nm SNP (**a**), 140 nm PSL, 30 nm SNP (**b**), 170 nm PSL, 30 nm SNP (**c**), 100 nm PSL, 10 nm SNP (**d**), 140 nm PSL, 10 nm SNP (**f**) and 170 nm PSL, 10 nm SNP (**f**). **g**, Reconstruction of 3D FIB-SEM tomography data. **h**, Surface rendering of the reconstructed volume showing the hexagonal arrangement of the supracolloids. **i**, FIB-SEM cross-section showing the arrangement of SNPs that fill the interstitial spaces between the PSL spheres. **j**, High magnification from the same region as in **i**. **k**, SEM image showing the hierarchical ordering of the SNPs in the dried material. **l**, High magnification from the same region as in **k**. **m**, FFT of the SEM image in **k** showing the hexagonal nano/meso arrangement of both the PSL spheres (information in the centre) and the SNPs (information in the highlighted circle). **n**, Inverse FFT of the highlighted area showing the hexagonal lattice of the SNPs. Scale bars, 1 μm.

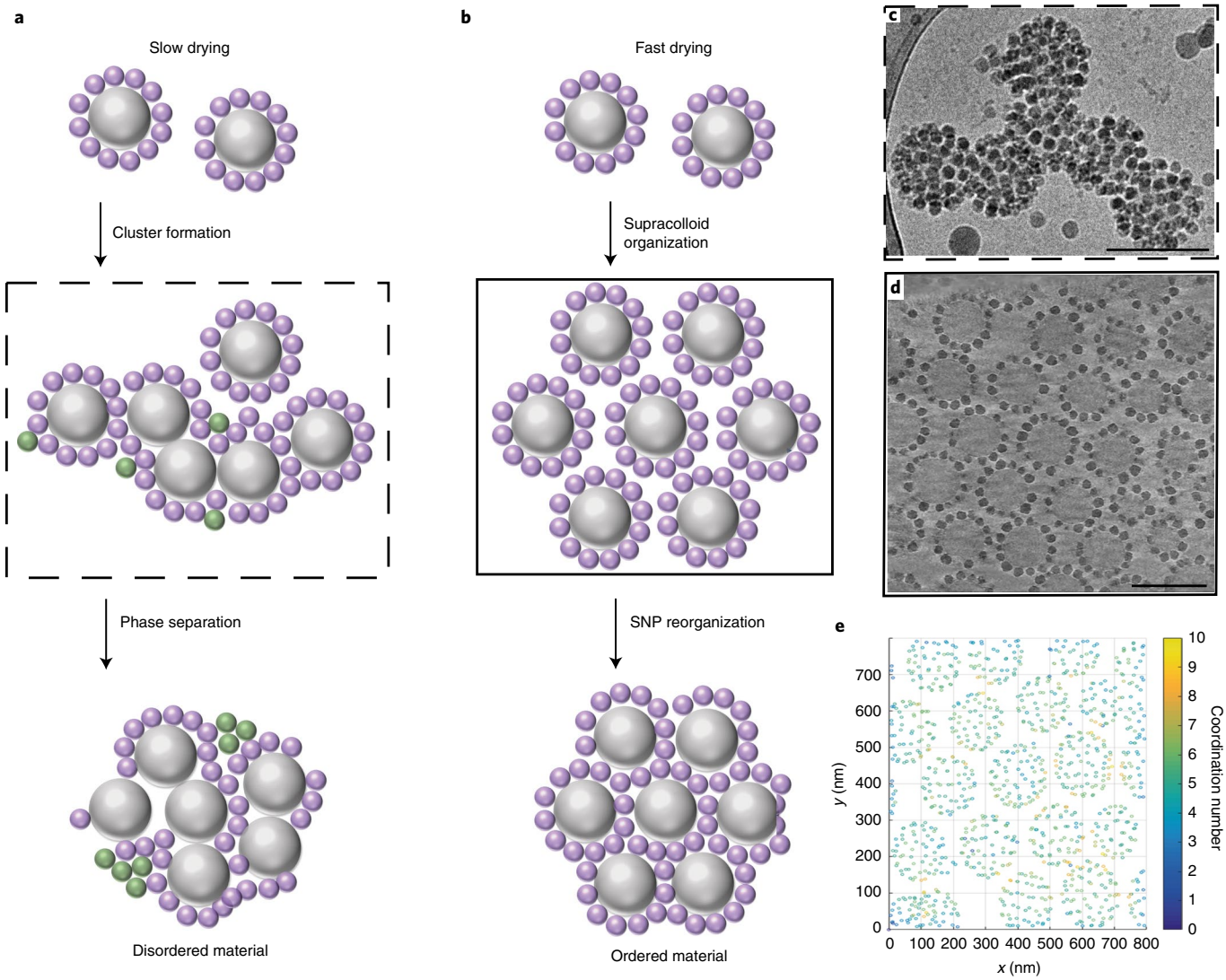

Fig. 3 | Analysis of the supracolloid 3D organization by cryoET. a,**b**, Schematic representation showing the rearrangement of the 30 nm SNPs at the 100 nm PSL surface during slow (**a**) and fast (**b**) drying. Although during slow drying rearrangements of the SNPs into secondary layers (shown in green) occurs, this effect is basically absent for fast drying. **c**, CryoTEM image of a supracolloid cluster formed in which SNPs rearranged during slow drying. **d**,**e**, *z* slice from the tomographic reconstruction of a non-clustering supracolloid sample in the concentrated regime during fast drying (**d**) and the coordination map for the SNPs in **d** showing the undisturbed surface packing (**e**). For details of the data analysis, see Supplementary Fig. 5. Scale bars, 200 nm.

of the above, zeta potential measurements showed that the overall charge of the supracolloids in Fig. 3 was +9 and +25 mV for the disordered and ordered systems, respectively. According to the Derjaguin–Landau–Verwey–Overbeek theory, higher zeta potential measurements correlate with particle stability[46,47], which indicates that forming supracolloids with higher total surface charges is essential to preserve the supracolloid integrity and avoid cluster formation. However, the overall charge on the supracolloids is not the only factor in determining structural evolution during concentration increase caused by drying. The drying time should be smaller than the reorganization time, to prevent the reorganization shown in Fig. 3a, but the repulsive forces between the supracolloids, decreasing with increasing ionic strength, should remain sufficiently present to promote the formation of the structure shown in Fig. 3b. Although most colloidal organization strategies involve drying samples as slowly as possible, in some case over several days[48], we observed that drying times of ~30 minutes resulted in ordered materials, whereas drying times longer than one hour resulted in disordered materials (Supplementary Table 3).

Modelling supracolloid formation and organization

We modelled the kinetics of the assembly process by considering how the relative concentration of each species evolves with time during the drying process (Fig. 4a). We considered a system of SNPs at a concentration S, which may stick to the PSL surfaces with N positions available on each PSL. The concentration of PSL spheres with n SNPs stuck to it is P_n. The formation of a PSL particle covered with n SNPs can be due to adsorption of an SNP on a PSL particle covered with $n-1$ SNPs, as described by a rate constant k_f, or desorption of an SNP from an PSL particle covered with $n+1$ SNPs as described by a rate constant k_b. Adsorption requires the proximity of an SNP and PSL particle covered with $n-1$ SNPs, so that the rate of formation is second order. Desorption depends only on the PSL spheres covered with $n+1$ SNPs and is thus first order. As in the simulations drying is not taken explicitly into account, for simplicity this effect was incorporated by taking cluster formation as irreversible with rate constant k_d. For simplicity and to limit the number of parameters within the model, the rate constants k_f, k, and

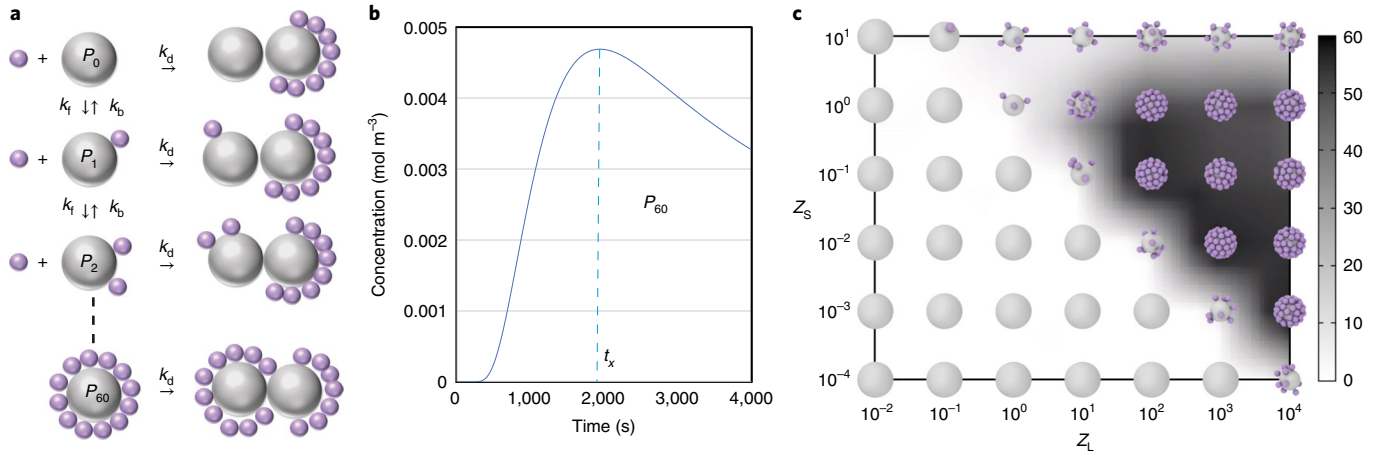

Fig. 4 | Modelling and optimization of the colloidal organization process. a, Schematic of the assembly reaction network showing the various pathways to ordered and disordered materials of 100 nm PSL and 30 nm SNP. **b**, Concentration of P_{60} versus time according to the population balance from equations (1) and (2), which shows the maximum at t_x = ~1,800 s. In this example the parameter values used were $P_0(0) = 1\,\mathrm{mol\,m^{-3}}$, $S(0) = 1\,\mathrm{m^{-3}}$, $k_f = 1\,\mathrm{m^3\,s^{-1}\,mol^{-1}}$, $k_b = 1\,\mathrm{s^{-1}}$ and $k_d = 0.001\,\mathrm{m^3\,s^{-1}\,mol^{-1}}$. **c**, Phase diagram generated by Monte Carlo simulations of the binary assemblies for a range of charge numbers of the small and large spheres, Z_S and Z_L. The background is coloured according to the number of SNPs on the surface of the supracolloids.

k_d were assumed to be independent of the number of SNPs on the composite particles.

The population balance equations for a composite particle of n small SNPs surrounding a PSL are given by:

$$\frac{dP_n}{dt} = k_f(P_{n-1} - P_n)S - k_b(P_n - P_{n+1}) - k_d P_n \sum_{i=0}^{N} P_i \quad (1)$$

$$\frac{dS}{dt} = -k_f S \sum_{i=0}^{N-1} P_i + k_b \sum_{i=1}^{N} P_i \quad (2)$$

Measuring all these rate constants, especially during drying, in which the solution conditions (concentration, ionic strength, pH and so on) continuously change would be extremely challenging. However, it is clear that the concentration of fully covered PSL spheres (P_{max}) goes through a maximum at time t_x (Fig. 4b), where x is dependent on k_f, k_b and k_d, and t_x indicates the time that corresponds to the maximum concentration of P_{max} in the system. In the simulation we assumed that $P_{max} = P_{60}$. To achieve the supracolloid morphology shown in Fig. 3c, the drying time should be optimized to coincide with t_x. In particular, sufficient repulsion between the supracolloids should remain present until they are fixed in a hexagonal pattern, in which some reorganization can take place and lead to a single layer of SNPs between PSL spheres.

To develop basic design rules for the formation of the supracolloids, Monte Carlo simulations were performed by considering the solution as a binary mixture of hard spheres with diameters σ_1 and σ_2 and a positive and negative surface charge density, which interact via a Yukawa potential[49], to account for the screening effect of the salts in solution. The two particles of species i and j interact via the potential:

$$\beta U(r_{ij}) = \begin{cases} \infty & r_{ij} \le \sigma_{ij} \\ \beta A_{ij} \frac{e^{-\kappa r_{ij}}}{(r_{ij}/\sigma_1)}, & \sigma_{ij} < r_{ij} \le r_c \\ 0 & r_{ij} > r_c \end{cases} \quad (3)$$

with $\beta = 1/k_B T$ (T is the temperature of the solvent), $\kappa = 1/\lambda_D$ (λ_D is the Debye screening length in solution) and r_{ij} is the distance between the particles. Also, the potential is cut at a cutoff distance r_c equal to $5\lambda_D$.

In particular, the amplitude of the potential A_{ij} depends on the surface charge of the species as:

$$\beta A_{ij} = \frac{\lambda_B}{\sigma_1} \frac{Z_i Z_j}{(1 + k\sigma_i/2)(1 + k\sigma_j/2)} e^{k\frac{\sigma_i + \sigma_j}{2}} \quad (4)$$

where λ_B is the Bjerrum length, and Z_i and Z_j are the charge numbers of the two species. To study the aggregation process of SNPs onto the surface of the PSL, we set up a simulation box with one PSL fixed in the centre of the box and SNPs free to move in the simulation box. We started the simulation at high temperatures, at which the SNPs are free to diffuse due to thermal agitation. Simulated annealing by quenching the system to lower and lower temperatures then triggered its energy-driven aggregation process and at temperature $T \simeq 0$ provided extremely low-energy states of the system of one PSL and many SNPs (Supplementary Video 2). We performed the aggregation study for many different values of the particle charges and determined the final cluster structures, which resulted in a state diagram as a function of charge numbers of the small and large particles, Z_S and Z_L, respectively, for the design of the supracolloids (Fig. 4c). Using this state diagram, it is synthetically simple to optimize the supracolloid morphology for our strategy towards hybrid materials, as the respective surface charges on the individual particles can easily be tuned using surface chemistry and solution conditions.

Outlook

Here we present the design and formation of hierarchically ordered materials through the colloidal assembly of spherical binary supracolloids using a general strategy that can be extended to colloidal systems with more components or even non-spherical building blocks. Intrinsic to this design is that enthalpic interactions cause the formation of the supracolloids, which subsequently self-assemble into 3D ordered structures driven by entropy, whereafter some rearrangements driven by enthalpy can occur. This two-step mechanism requires a subtle balance of the particle size ratio, energetic interactions (dictated by the surface chemistry and solution conditions) and the kinetics of the drying process. In addition, it is important that the dynamic nature of the supracolloids is maintained during the hierarchical self-assembly process and that phase separation and stratification are avoided. Given the versatility of colloidal

self-assembly and the simple design rules provided here to optimize the system, we anticipate that this fundamental approach will lead to new hierarchical hybrid materials, which benefit from a modular building block assembly. The redefinition of the building block at different scales will be key to move from hybrid materials to multicomponent and multiscale hierarchies. High-surface-area materials in absorption, catalysis and multicomponent nanostructures with a controlled flow in porous media are potential applications for these well-controlled materials.

Online content

Any methods, additional references, Nature Research reporting summaries, source data, extended data, supplementary information, acknowledgements, peer review information; details of author contributions and competing interests; and statements of data and code availability are available at https://doi.org/10.1038/s41563-020-00900-5.

Received: 19 October 2019; Accepted: 4 December 2020;
Published online: 28 January 2021

References

1. O'Brien, M. N., Jones, M. R. & Mirkin, C. A. The nature and implications of uniformity in the hierarchical organization of nanomaterials. *Proc. Natl Acad. Sci. USA* **113**, 11717–11725 (2016).
2. Boles, M. A., Engel, M. & Talapin, D. V. Self-assembly of colloidal nanocrystals: from intricate structures to functional materials. *Chem. Rev.* **116**, 11220–11289 (2016).
3. Vogel, N., Retsch, M., Fustin, C. A., Del Campo, A. & Jonas, U. Advances in colloidal assembly: the design of structure and hierarchy in two and three dimensions. *Chem. Rev.* **115**, 6265–6311 (2015).
4. Gerth, M. & Voets, I. K. Molecular control over colloidal assembly. *Chem. Commun.* **53**, 4414–4428 (2017).
5. Elacqua, E., Zheng, X., Shillingford, C., Liu, M. & Weck, M. Molecular recognition in the colloidal world. *Acc. Chem. Res.* **50**, 2756–2766 (2017).
6. Chen, Q., Bae, S. C. & Granick, S. Directed self-assembly of a colloidal kagome lattice. *Nature* **469**, 381–384 (2011).
7. Leunissen, M. E. et al. Ionic colloidal crystals of oppositely charged particles. *Nature* **437**, 235–240 (2005).
8. Hueckel, T., Hocky, G. M., Palacci, J. & Sacanna, S. Ionic solids from common colloids. *Nature* **580**, 487–490 (2020).
9. Ben Zion, M. Y. et al. Self-assembled three-dimensional chiral colloidal architecture. *Science* **358**, 633–636 (2017).
10. Mirkin, C. A., Letsinger, R. L., Mucic, R. C. & Storhoff, J. J. A DNA-based method for rationally assembling nanoparticles into macroscopic materials. *Nature* **382**, 607–609 (1996).
11. Hynninen, A. P., Christova, C. G., van Roij, R., van Blaaderen, A. & Dijkstra, M. Prediction and observation of crystal structures of oppositely charged colloids. *Phys. Rev. Lett.* **96**, 138308 (2006).
12. Frenkel, D. & Ladd, A. J. C. New Monte-Carlo method to compute the free-energy of arbitrary solids—application to the FCC and HCP phases of hard-spheres. *J. Chem. Phys.* **81**, 3188–3193 (1984).
13. van Blaaderen, A., Ruel, R. & Wiltzius, P. Template-directed colloidal crystallization. *Nature* **385**, 321–324 (1997).
14. de Nijs, B. et al. Entropy-driven formation of large icosahedral colloidal clusters by spherical confinement. *Nat. Mater.* **14**, 56–60 (2015).
15. Zeng, X. et al. Supramolecular dendritic liquid quasicrystals. *Nature* **428**, 157–160 (2004).
16. Ungar, G., Liu, Y., Zeng, X., Percec, V. & Cho, W. D. Giant supramolecular liquid crystal lattice. *Science* **299**, 1208–1211 (2003).
17. Damasceno, P. F., Engel, M. & Glotzer, S. C. Predictive self-assembly of polyhedra into complex structures. *Science* **337**, 453–457 (2012).
18. Lenz, M. & Witten, T. A. Geometrical frustration yields fiber formation in self-assembly. *Nat. Phys.* **13**, 110–1104 (2017).
19. Wang, P. Y. & Mason, T. G. A Brownian quasi-crystal of pre-assembled colloidal Penrose tiles. *Nature* **561**, 94–99 (2018).
20. Lee, S., Bluemle, M. J. & Bates, F. S. Discovery of a Frank–Kasper sigma phase in sphere-forming block copolymer melts. *Science* **330**, 349–353 (2010).
21. Glotzer, S. C. & Solomon, M. J. Anisotropy of building blocks and their assembly into complex structures. *Nat. Mater.* **6**, 557–562 (2007).
22. de Graaf, J., van Roij, R. & Dijkstra, M. Dense regular packings of irregular nonconvex particles. *Phys. Rev. Lett.* **107**, 155501 (2011).
23. Dijkstra, M. Entropy-driven phase transitions in colloids: from spheres to anisotropic particles. *Adv. Chem. Phys.* **156**, 35–71 (2015).
24. Talapin, D. V. et al. Quasicrystalline order in self-assembled binary nanoparticle superlattices. *Nature* **461**, 964–967 (2009).
25. Shevchenko, E. V., Talapin, D. V., Kotov, N. A., O'Brien, S. & Murray, C. B. Structural diversity in binary nanoparticle superlattices. *Nature* **439**, 55–59 (2006).
26. Kim, M. H., Im, S. H. & Park, O. O. Fabrication and structural analysis of binary colloidal crystals with two-dimensional superlattices. *Adv. Mater.* **17**, 2501–2505 (2005).
27. Friedrich, H. et al. Quantitative structural analysis of binary nanocrystal superlattices by electron tomography. *Nano Lett.* **9**, 2719–2724 (2009).
28. Evers, W. H. et al. Entropy-driven formation of binary semiconductor–nanocrystal superlattices. *Nano Lett.* **10**, 4235–4241 (2010).
29. Evers, W. H., Friedrich, H., Filion, L., Dijkstra, M. & Vanmaekelbergh, D. Observation of a ternary nanocrystal superlattice and its structural characterization by electron tomography. *Angew. Chem. Int. Ed.* **48**, 9655–9657 (2009).
30. Singh, G., Pillai, S., Arpanaei, A. & Kingshott, P. Layer-by-layer growth of multicomponent colloidal crystals over large areas. *Adv. Funct. Mater.* **21**, 2556–2563 (2011).
31. Subramanian, G., Manoharan, V. N., Thorne, J. D. & Pine, D. J. Ordered macroporous materials by colloidal assembly: a possible route to photonic bandgap materials. *Adv. Mater.* **11**, 1261–1265 (1999).
32. Subramania, G., Constant, K., Biswas, R., Sigalas, M. M. & Ho, K.-M. Optical photonic crystals fabricated from colloidal systems. *Appl. Phys. Lett.* **74**, 3933–3935 (1999).
33. Chai, G. S., Shin, I. S. & Yu, J.-S. Synthesis of ordered, uniform, macroporous carbons with mesoporous walls templated by aggregates of polystyrene spheres and silica particles for use as catalyst supports in direct methanol fuel cells. *Adv. Mater.* **16**, 2057–2061 (2004).
34. Meng, Q. B. et al. Assembly of highly ordered three-dimensional porous structure with nanocrystalline TiO_2 semiconductors. *Chem. Mater.* **14**, 83–88 (2002).
35. Cho, Y.-S. et al. Self-organization of bidisperse colloids in water droplets. *J. Am. Chem. Soc.* **127**, 15968–15975 (2005).
36. Chen, Q. et al. Supracolloidal Reaction Kinetics of Janus Spheres. *Science* **331**, 199–202 (2011).
37. Hsiao, L. C. & Pradeep, S. Experimental synthesis and characterization of rough particles for colloidal and granular rheology. *Curr. Opin. Colloid Interface Sci.* **43**, 94–112 (2019).
38. Harley, S., Thompson, D. W. & Vincent, B. The adsorption of small particles onto larger particles of opposite charge. Direct electron microscope studies. *Colloids Surf.* **62**, 163–176 (1992).
39. De Silva Indrasekara, A. S. et al. Tailoring the core–satellite nanoassembly architectures by tuning internanoparticle electrostatic interactions. *Langmuir* **34**, 14617–14623 (2018).
40. Patterson, J. P., Xu, Y., Moradi, M. A., Sommerdijk, N. & Friedrich, H. CryoTEM as an advanced analytical tool for materials chemists. *Acc. Chem. Res.* **50**, 1495–1501 (2017).
41. Evans, J. W. Random and cooperative sequential adsorption. *Rev. Mod. Phys.* **65**, 1281–1329 (1993).
42. Manoharan, V. N. Colloidal matter: packing, geometry, and entropy. *Science* **349**, 1253751 (2015).
43. Bausch, A. R. et al. Grain boundary scars and spherical crystallography. *Science* **299**, 1716–1718 (2003).
44. Guerra, R. E., Kelleher, C. P., Hollingsworth, A. D. & Chaikin, P. M. Freezing on a sphere. *Nature* **554**, 346 (2018).
45. Keddie, J. & Routh, A. F. Fundamentals of Latex Film Formation: Processes and Properties. *Springer Science & Business Media,* (2010).
46. Verwey, E. J. Theory of the stability of lyophobic colloids. *J. Phys. Colloid Chem.* **51**, 631–636 (1947).
47. Derjaguin, B. & Landau, L. Theory of the stability of strongly charged lyophobic sols and of the adhesion of strongly charged-particles in solutions of electrolytes. *Prog. Surf. Sci.* **43**, 30–59 (1993).
48. Cong, H. & Yu, B. Fabrication of superparamagnetic macroporous Fe3O4 and its derivates using colloidal crystals as templates. *J. Colloid Interface Sci.* **353**, 131–136 (2011).
49. Robbins, M. O., Kremer, K. & Grest, G. S. Phase-diagram and dynamics of Yukawa systems. *J. Chem. Phys.* **88**, 3286–3312 (1988).
50. Mansfield, M. L. The random parking of spheres on spheres. *J. Chem. Phys.* **105**, 3245 (1996).

Methods

Materials. Aqueous suspensions of PSL spheres were obtained from either Sigma-Aldrich (LB1) or Fisher Scientific (Distrilab) and used as received. For the size-effect experiments, we used 110 nm (standard deviation 14 nm, volume concentration 10%) PSL spheres (Aldrich) with 0.1% sodium azide preservative and surfactant, 140 nm PSL spheres (volume concentration <5%) and 170 nm PSL spheres (volume concentration <6%) with a trace amount of surfactant. L-lysine was supplied by Fluka and tetraethyl orthosilicate was obtained from VWR. APTES was ordered from Merck (Sigma-Aldrich). pH buffers were prepared as shown in Supplementary Table 1.

Synthesis of SNPs. SNPs were synthesized using the Yokoi method[51], employing a similar procedure to that of Carcouët et al.[51]. L-lysine (100 mg; Fluka) was dissolved in pure water (100 ml) in a three-neck 250 ml flask, and the reaction solution was magnetically stirred (270 r.p.m.) at 60 °C under reflux. Later, the reaction was initiated by adding tetraethyl orthosilicate (6 ml for 30 nm SNPs and 0.6 ml for 10 nm SNPs; VWR) in one swift motion to the reaction solution. The reaction was terminated after 24 h (ref. [52]). For 30 nm SNPs, size measurement of the resulting particles by dynamic light scattering (ZetaNano) gave a Z average diameter of 31 nm and an intensity averaged particle diameter of 35 nm. CryoTEM imaging and analysis showed an approximate size of about 26 nm. For 10 nm particles, dynamic light scattering gave a Z average diameter of 11 nm and an intensity averaged particle diameter of 13 nm. CryoTEM analysis indicated an approximate size of about 9 nm.

Surface functionalization of silica nanoparticles. The colloidal silica suspension was diluted to 10 wt% (pH ~9), and a 1 wt% silane solution in water (pH ~11) was slowly added with vigorous stirring. The initial amount of APTES and colloidal silica used was such that the silane:silica weight ratio was kept at 1:200, above which the particles rapidly coagulated. The silane:silica mixture was then washed by repeated centrifugation and replacement of the supernatant at least five times. Ultrapure water (resistivity 18 MΩ cm by Milli-Q water purifier) was used in all the experiments[53].

Self-assembly of supracolloids. A stock dispersion was prepared by diluting PSL 1:10 with water. The added buffer volume was calculated based on the desired ionic strength for the specific sample volume (Supplementary Table 1). The remaining sample volume was then split between the PSL stock dispersion and a (modified) SNP solution to a $V_{SNP}/V_{PSL} = 0.8$ ratio. About seven days after mixing, 0.1–10 µl was taken to deposit as a droplet on the desired substrate for controlled drying experiments.

CryoTEM and cryoET. CryoTEM samples were prepared by depositing 3 µl samples on a 200 mesh Cu grid with a Quantifoil R2/2 holey carbon film (Quantifoil Micro Tools GmbH) or lacey carbon 200 mesh (Electron Microscopy Sciences). All the TEM grids were surface plasma treated for 40 s using a Cressington 208 carbon coater prior to use. An automated vitrification robot (Fisher Scientific Vitrobot Mark III) was used for plunge vitrification in liquid ethane. CryoTEM studies were performed on a TU/e cryoTITAN (Thermo Fisher Scientific) operated at 300 kV, equipped with a field emission gun, a postcolumn Gatan energy filter and a post-Gatan energy filter 2k×2k Gatan charge-coupled device camera. Images were recorded with a total electron flux of less than 100 e^- Å^{-2}. Matlab scripts developed in-house were used for image analysis. The electron tomography tilt series was taken by tilting the specimen from −65 to 65°, at 2 or 3° per step with Inspect 3D software (Thermo Fisher Scientific). The alignment and 3D reconstruction of the tilt series were done by using IMOD software using SNPs as fiducials or by patch tracking and reconstructed using SIRT (simultaneous iterative reconstruction technique) with 10–40 iterations. The images were taken at 6,500, 11,500 and 19,000 times the nominal magnification, with a pixel size of 1.4, 0.76 and 0.47 nm, respectively. The nominal defocus during data acquisition was set to −10, −5 and −2 µm, respectively. The total dose for the acquisition was approximately 100 e^- Å^{-2}. Subsequently, in some cases, data were denoised by non-linear anisotropic diffusion prior to visualization. The resultant 3D reconstructions are shown in Supplementary Videos 3 and 4[54].

Analysis of supracolloid organization from tomographic data. To quantitatively analyse the SNP arrangements on the surface of silica particles, we performed image analysis on the cryoET data of several samples and applied the following steps to extract the positional data and neighbouring networks of the SNPs. For the associated tilt series and the 3D reconstruction, see Supplementary Video 3. Template matching of the spheres was used to determine the position of the silica particles in an inversed contrast tomogram of the supracolloids or dried materials. The inversed contrast was calculated to minimize the background signal, and thus increase the signal-to-noise ratio, which results in a more reliable template matching for the SNP in the 3D image.

Step 1: find probable PSL centres. The input for this step is a list of *xyz* coordinates of the SNP centres, displayed in Supplementary Fig. 1a. The first step was to make an *xyz* grid that covered all the silica centres. Next, for every point on the grid, the distances to all the other SNP centres were calculated. After that, for every grid point, the amount of SNPs between a minimum and maximum distance was counted. The grid points that have at least a minimum amount of silica particles were selected; the rest were discarded. The results of the selected centres are displayed in Supplementary Fig. 1b.

Step 2: locate centres of the probable PSL clusters. From the clusters of SNPs, probable PSL centre locations of a single value are desired. This was done using MATLAB's region props. In some cases, we needed to decide manually because sometimes two locations were found for a single PSL particle. The results are shown in Supplementary Fig. 1c.

Step 3: find the radius and corrected centres. For every found PSL particle, all the SNPs in a 110 pixel radius (corresponding to the expected PSL radius plus the diameter of an SNP) were used. The SNPs were fitted on a sphere using the least-squares method. In some cases, the fitted radius may be smaller than 110 pixels, and the correlated centre may differ as well compared with the centre located in step 2. That is why the sphere should be refitted using the points that are close to the new centre and within the new radius times a margin. This iteration can be repeated many times. The resultant fitted spheres are shown in Supplementary Fig. 1d.

Step 4: dividing the silica particles over the PSL centres. In the next step, the SNPs were divided over the PSL centres based on the distance to the centre. In general, the SNP point was connected to the closest PSL point, but in exceptional cases the distance was irrationally long. When these points were successfully divided over the PSL centres, an alpha shape can be made. The alpha shapes are displayed in Supplementary Fig. 1e.

Step 5: including unresolved points. Some of the SNP particles may not be connected to PSL particles. In most cases, these SNPs were on the borders of the 3D coordinates and far away from PSL particles. However, in some cases, the particles were close to a PSL particle, and it is possible that these SNP particles were included in the alpha shapes manually. After finding all the SNPs that belong to one supracolloid particle, we calculated the nearest-neighbour distance and nearest-neighbour network for each SNP–PSL particle. We could then calculate the coordination numbers followed by a coordination map on each supracolloidal particle, as shown in Supplementary Fig. 5.

Data availability

The data that support the findings of this study are available within the article and Supplementary Information files and from the corresponding authors upon reasonable request (see 'Author contributions' for the specific datasets). Source data are provided with this paper.

Code availability

Code for the analysis of the tomographic reconstructions is available from M.-A.M. upon request. Code for the Monte Carlo simulations is available from M.D. upon request. Code for the population balance modelling is available from A.F.R. upon request.

References

51. Yokoi, T. et al. Periodic arrangement of silica nanospheres assisted by amino acids. *J. Am. Chem. Soc.* **128**, 13664–13665 (2006).
52. Carcouët, C. C. M. C. et al. Nucleation and growth of monodisperse silica nanoparticles. *Nano Lett.* **14**, 1433–1438 (2014).
53. Pham, K. N., Fullston, D. & Sagoe-Crentsil, K. Surface charge modification of nano-sized silica colloid. *Aust. J. Chem.* **60**, 662–666 (2007).
54. McKenzie, B. E. et al. Controlling internal pore sizes in bicontinuous polymeric nanospheres. *Angew. Chem. Int. Ed. Engl.* **54**, 2457–2461 (2015).

Acknowledgements

We thank I. Schreur-Piet (Eindhoven University of Technology) for her help with the FIB/SEM TEM lamella sample preparation and P. Bomans (Eindhoven University of Technology) for his support with the CryoTEM. E.D.E. and M.C. were supported by the EU H2020 Marie Sklodowska-Curie Action project 'MULTIMAT'. J.P.P. and M.-A.M. were supported by the 4TU High-Tech Materials research programme 'New Horizons in Designer Materials'.

Author contributions

N.S., H.F., M.-A.M., E.D.E. and J.P.P. conceived and designed the experiments. M.-A.M. and E.D.E. carried out the supracolloid assembly experiments. M.-A.M. carried out the cryoTEM and cryoET analysis. E.D.E. carried out the SEM analyses and FIB experiments. M.D. supervised the simulation study and M.C. carried out the computer simulations. S.R. carried out the silica functionalization and some of the drying experiments. H.F. supervised the data analysis and M.-A.M., E.D.E., M.G. and A.D.A.K.

carried out the data analysis. M.M.J.v.R. synthesized the SNPs. A.F.R. created the kinetic model. N.A.J.M.S., G.d.W., H.F. and J.P.P. supervised the project. J.P.P. wrote the manuscript and M.-A.M., E.D.E. and G.d.W. wrote the Supplementary Information, with contributions from all the authors. All the authors discussed the results and commented on the manuscript.

Competing interests

The authors declare no competing interests.

Additional information

Supplementary information is available for this paper at https://doi.org/10.1038/s41563-020-00900-5.

Correspondence and requests for materials should be addressed to N.S., H.F. or J.P.P.

Peer review information *Nature Materials* thanks Dganit Danino, Oleg Gang and the other, anonymous, reviewer(s) for their contribution to the peer review of this work.